UNIVERSITÀ DEGLI STUDI DI FIRENZE

DIPARTIMENTO DI INGEGNERIA ELETTRONICA

A "REAL TIME" TWO-DIMENSIONAL PULSED WAVE DOPPLER SYSTEM

Marco Calzolai, Lorenzo Capineri, Ada Fort, Leonardo Masotti, Marco Scabia

RAPPORTO INTERNO # 981101 – Novembre 1998

50139 FIRENZE (ITALY) – Via S. Marta, 3 – Tel. 47961 Telex 572460 Unifi

Introduction

The reconstruction of blood motion inside vessels of the human body is still one of the most ambitious goals of medical imaging systems. Doppler ultrasound (Evans et al. 1989) and Magnetic Resonance Angiography (Mohiaddin et al.1994) can be employed *in vivo* to measure the velocity profile of blood. Ultrasound methods play an important role for their well known safety and for the limited cost of diagnostic equipments. Today, the investigation of vascular diseases is usually performed with ultrasound scanners which are based on the measurement of Doppler shift on a transmitted probing signal reflected from a sample volume of the moving blood. Besides the great importance of Doppler ultrasound in clinical routine, this method is limited to measure only the blood velocity component along the direction of the transmitting probe ultrasonic beam. True velocity profiles can be obtained only when the beam to flow angle is known and quantitative investigation of hemodynamics becomes more difficult in presence of complex flows generated by stenosis or in proximity of a vessel bifurcation.

An emerging technique, called *multidimensional Doppler*, is based on the possibility of a sample volume illumination along different directions: this method can be exploited to overcome the limitation of the single beam Doppler method because the true velocity vector associated to the sample volume can be estimated through the vector components. The idea of vector velocity estimation was proposed by several authors and different techniques were experimented for its application in two and three dimensions based on different methods: multiple beam transducers (Overbeck et al. 1992; Hein 1994; Bruni et al. 1995, Phillips et al. 1996), spectral broadening (Newhouse et al. 1987), transverse spatial modulation (Jensen and Munk1998) and speckle tracking (Thraey et al. 1987).

Multidimensional Doppler can also benefit from new developments of echographic systems with real-time three-dimensional (3D) scanning capability. Matrix array of transducers with electronic focussing and steering (Smith et al. 1991) and mechanical scanning with a probe mounted on a gyroscopic movement (Masotti and Pini 1992, Pini et al. 1993, Shandas et al. 1998) can effectively investigate a volume inside the body. At present they are not yet widely employed in commercial echographs due to their high manufacturing cost but we can foresee their availability in a near future since a lot of interest is put in research of 3D scanners (Emery and Smith 1997).

In this context our work is addressed to the development of a two-dimensional Pulsed Wave (PW) Doppler system capable to generate real-time images of the projection of the velocity vector field over the scanning plane. An electronic interface between a personal computer and a

commercial echograph (ESAOTE AU-3 Partner) was designed to have the external control of the focusing and steering electronics of a 128 elements linear array and in order to add a new operating mode performing two-dimensional Doppler measurements over a user defined area. Though a two-dimensional system is simpler than a three-dimensional one, for its implementation in real-time was necessary to tackle several design problems:

1. Multidimensional scanning strategy
2. Digital signal processing for filtering and baseband demodulation
3. Visualisation of the vector field in real-time
4. Audio output.

The extension of the Doppler investigation from one to two and three dimensions requires new methods of presentation of the measured velocity vector field. In a monodimensional Doppler system, this information is treated in different ways to produce intelligible outputs in real-time to the physician for diagnosis. Typically the instrument provides an audio output, a spectrogram display and, in more advanced system, a color flow mapping (CFM). The latter technique represents the effort to extend the monodimensional Doppler to the investigation over a large area of the vessel section and extensive studies have been published on the clinical relevance of CFM images (Ferrara and De Angelis 1997). An ultrasonic scanner operating in CFM mode has the advantage to show qualitative information of blood flow in real-time and to correlate them to the vessel morphology by superposing the velocity color map on a (B-scan) grey scale image. Among other limitations also the CFM suffers from angle dependence as it is derived from the monodimensional Doppler method.

The development of a multidimensional Doppler ultrasound instrument for quantitative evaluation of non stationary flows could improve the reliability and the versatility of diagnosis in vascular diseases. This new approach should stimulate the research of novel diagnostic tools able to detect vascular disease by processing vector velocity maps provided by a multidimensional Doppler system. In this work we present the basic principle of operation of the two-dimensional Doppler technique, a real-time visualisation method of the measured vector field, the characteristics of the designed prototype instrument and finally the results obtained with measurements on laboratory test-objects and an example of the carotid artery flow *in vivo*.

2. Two dimensional Doppler technique

Multidimensional Doppler techniques make use of multiple transducers in order to perform Doppler measurements along different lines of sight, over the same investigated volume.

In this work we present the design of a new system to perform 2D Doppler measurements, based on a 128 elements linear array transducer with electronic focussing and beam steering. The method employs portions of the array to obtain sub-apertures and perform Doppler measurements along two different directions.

As shown in figure 1, the velocity measurement on a voxel at depth Z_0 is performed by using a central sub-aperture, which operates as transmitter (TX) with a steering angle 0°, and two lateral receivers (RX_1 and RX_2), with steering angles θ_1= +12° and θ_1= -12° respectively. In order to reduce errors on the velocity estimate, the steering angles were chosen as the maximum allowed by the beam-former in the ESAOTE AU-3 echograph used to develop the 2D Doppler system.

Figure 1: Linear array with transmitter (TX) and receiver (RX_1 and RX_2) sub-apertures for two-dimensional Doppler measurements. The linear array probe scanning plane is at y=0 and the measured component velocity on this plane is (vettore)v_{XZ}

The 2D vector velocity estimate is performed as follows; considering the situation shown in figure 1, the Doppler shifts f_1 and f_2, measured by the two receivers RX_1 and RX_2 respectively, are given by:

$$f_1 = -f_t(\underline{v} \cdot \underline{i}_0 + \underline{v} \cdot \underline{i}_1)/c \qquad (1)$$
$$f_2 = -f_t(\underline{v} \cdot \underline{i}_0 + \underline{v} \cdot \underline{i}_2)/c$$

where $\underline{v} = (v_x, v_y, v_z)$ is the velocity vector, f_t is the central frequency of the transmitted burst, c is the velocity of sound, and $\underline{i}_0=(0,0,1)$, $\underline{i}_1=(\sin\theta_1,0,\cos\theta_1)$, $\underline{i}_2=(\sin\theta_2,0,\cos\theta_2)$ are unity vectors indicated in figure 1.

By the set of equations in (1), it's possible to determine the two components of v_x and v_z:

$$v_z = (c/f_t)(f_2 \sin\theta_1 - f_1 \sin\theta_2)/(\sin\theta_2 (1+\cos\theta_1) - \sin\theta_1 (1+\cos\theta_2)) \qquad (2)$$
$$v_x = (c/f_t)(f_2 (1+\cos\theta_1) - f_1 (1+\cos\theta_2))/(\sin\theta_2 (1+\cos\theta_1) + \sin\theta_1 (1+\cos\theta_2))$$

In our system both receivers RX_1 and RX_2 have the same distance D from the transmitter TX, consequently assuming a fixed steering angle $\theta_S = \theta_1 = -\theta_2 = 12°$, it is possible to demonstrate by simple geometrical considerations that the two receiver directions $\underline{i}_1$, and $\underline{i}_2$ intersect the direction $\underline{i}_0$ in the same point P at depth Z_0; this working condition simplifies equations (2) to:

$$v_z = -(c/2f_t)(f_1 + f_2) / (1 + \cos\theta_S) \quad (3)$$

$$v_x = (c/2f_t)(f_2 - f_1) / \sin\theta_S$$

Therefore we can measure the projection of velocity vector $\underline{v}$ on the scan plane (y=0)of the linear array using equations (2) and (3).

The 2D Doppler system calculates Doppler shifts f_1 and f_2 as centroids of the Fast Fourier Transforms (FFT) of the demodulated Doppler signals from receivers RX_1 and RX_2. FFT estimation is carried out by using the periodogram technique (Oppenheim and Shafer 1985). Centroid calculations are carried out on those portions of the Doppler normalized spectra which are above a programmable threshold.

As in common PW Doppler systems a maximum depth of investigation Z_{MAX} can be defined as a function of Pulse Repetition Frequency (PRF); in the 2D Doppler case with the above assumptions for the scanning geometry, the round trip distance is $Z_{MAX}(1+\cos\theta_S)$, and therefore Z_{MAX} depends on θ according to the following relationship:

$$Z_{MAX} = (c / PRF)(\cos\theta_S / (1+\cos\theta_S)) \quad (4)$$

We can observe that equation (4) when $\theta_S = 0$, reduces to the well known result for the monodimensional Doppler which is $Z_{MAX} = c / (2\,PRF)$.

Another important issue in Doppler systems that operate in PW mode is the aliasing problem.

In the case of 2D Doppler the maximum detectable velocity still depends on the PRF and the angle between the probe axis and the velocity vector but with a different law than in the monodimensional case. In 2D Doppler the maximum detectable velocity is different for the two receivers, as they receive the scattered signal from the same voxel with different angles. The relationships reported below (eq. 5) determine the maximum velocity module v_{XZ} detectable by receivers 1 and 2 as a function of PRF and the steering angle θ_S:

(5)

$$[v_{xz}]_{MAX\_RX1} = \frac{c}{f_t} \cdot \left| \frac{PRF}{2(\beta - 1)} \right| \cdot \sqrt{\frac{1}{\sin^2\theta_s} + \frac{\beta^2}{(1+\cos\theta_s)^2}}$$

$$[v_{xz}]_{MAX\_RX2} = \frac{c}{f_t} \cdot \left| \frac{PRF}{2(\beta + 1)} \right| \cdot \sqrt{\frac{1}{\sin^2\theta_s} + \frac{\beta^2}{(1+\cos\theta_s)^2}}$$

where $\beta = \frac{1}{tg(\alpha)} \cdot \frac{1+\cos\theta_s}{\sin\theta_s}$ and $\theta_S = \theta_1 = -\theta_2$ and α are defined in Figure 1.

Finally the overall maximum velocity detectable is chosen as:

(6)

$$[v_{xz}]_{MAX} = \min \{ [v_{xz}]_{MAX\_RX1}, [v_{xz}]_{MAX\_RX2} \}$$

One of the advantages of operating in PW Doppler mode is the possibility to use the system to scan an area and to obtain a vector velocity map.
The technique used for lateral scan is done by moving the Tx-Rx group of sub-apertures along the array (figure 2) keeping constant the distance D between Tx and Rx.

Figure 2. Example of lateral scan with four lines of sight at fixed depth Z_o. The scan is done by moving the TX-RX_i group (i=1,2) of sub-apertures along the array. The distance D between TX and RX_i remains constant for a scan at fixed depth Z_o.

The axial scan instead, is obtained as a composition of two different scanning techniques; the first is used for a coarse spatial sampling and the second, based on multigate processing, for a finer spatial sampling.
The first most straightforward scanning technique, involves keeping fixed the TX sub-aperture position on the array, and moving symmetrically the two receivers RX_1 and RX_2 in opposite lateral directions, with constant steering angles.

Figure 3: Axial scanning methods for 2D PW Doppler: coarse axial sampling changing the distance D to D' between TX and RX_i ; fine sampling with multigate method.

The second axial scanning technique, involves the use of multigate: for each receiver a portion of the RF signal, divided in several sub-portions (gates), is acquired and processed. Each sub-portion provides the Doppler information from a different voxel.
Figure 3 shows an example of the combined application of the two techniques to investigate six equally spaced voxels: multigates 1 and 2, centered at depths Z_1 and Z2, provide Doppler measurements of voxels 1-2-3 and 4-5-6 respectively. In this example the gates duration is chosen as one third of the multigate duration.

Obviously the multigate technique can be used only for short depth ranges, since all the gates must fall close to the TX and RXi beam axes intersection. One advantage of the multigate technique is that it drastically reduces acquisition times, since it allows to perform Doppler measurements on more voxels in the same time required to measure a single voxel with the first technique. This is an important advantage because the 2D Doppler measurement over an area must be carried out in a time which is lower than the stationarity time of blood flow, which is about 20 ms.

The 2D Doppler system employs the described axial and lateral scan techniques to investigate a rectangular area; the user can select the size of this area as a tradeoff between acquisition time and size of the area.

Given the length of the array (128 elements, pitch 0.36mm), 32 elements for the subaperture and the steering angle 12°, the theoretical maximum area which is possible to investigate is the triangle represented in figure 4.

Figure 4: Theoretical maximum scanning area defined by the length of the array and the chosen steering angle θ_S=12°.

The area actually scanned will always be a smaller portion of the triangle shown in figure 4. An example of scanned area, formed by 10x10 voxels, is shown as a dotted rectangle in figure 4; this rectangle can be scanned in 100 ms, by using a 10 kHz PRF, with 16 PRF per voxel, two 10 lines lateral scans at depths Z_1 and Z_2 respectively, each containing 5 gates.

3. Visualisation methods for real-time 2D velocity vector fields

The visualization of vector fields relative to volumetric data is a common problem encountered in engineering and physical sciences. Multidimensional Doppler systems also need suitable visualization methods of the velocity vector field relative to a scanned volume with the additional problem of a real-time operation.

The general case refers to the visualization of a three-dimensional velocity vector field and it was tackled in a previous work by the authors with a 3D Doppler system capable of mechanical volume scanning, that operated off-line (M. Calzolai et al. 1996). In that work the data acquisition was carried out on a stationary velocity field generated by a laboratory test-object; the velocity field was visualized with a specifically developed software, with two different representations, a qualitative one to give an overall impression of flow distribution, and a quantitative one for more precise analysis.

For the present work a reduced version of this software was used to give a quantitative representation of a 2D flow in real-time. In the 2D case the problem of visualization is simpler than in 3D, but to give an intuitive reperesentation of the evolution of the 2D flow to the physician is still a challenging problem.

Other authors proposed imaging techniques based on colour coding of velocity vector information: Li (Li et al., 1997) and Ding-Yu (Ding-Yu et al., 1994) used two separated images to represent module and angle information with a color coding similar to that employed in CFM; Charles (Charles, 1989) and (Vera et al., 1992) used a HLS (Hue-Lightness-Saturation) color coding in order to represent both module and angle information in a single image. Theofanis (Theofanis et al., 1994) presented a method which used velocity vectors, superposed to the B-mode image, along selected directions but without colour coding. Another display method developed by Ding-Yu Fei et.al. superposed the velocity vectors to the color coded velocity module image.

In this work we propose two different visualisation methods aimed to make the interpretation of the vector image easier, by combining colour coding and graphical representation of vectors. The basic idea remains the superposition of both velocity vectors and the color coding to the B-scan image. Figure 5 shows an example of these two representations relative to the 2D Doppler acquisition on a Doppler thread phantom over a 12mm by 12 mm area (outlined by the yellow box). The representation in Fig.5A is the extension of the common CFM to the vector Doppler where each voxel is displayed with a color which indicates the velocity module. On each voxel center is displayed a vector in yellow which indicates the direction and module of the velocity estimated in that position.

The second type of visualisation, shown in Fig.5B, employs a graphical description of the flow by drawing only coloured vectors with length proportional to the velocity module and the same colour coding and application points used in Fig.5A.

As in CFM visualisation methods commonly used in echographic systems, the determination of which voxels must actually be displayed within the scanned area, is carried out by applying a threshold criteria on the backscattered energy from each voxel. Fig.6 shows the velocity field image, relative to the same acquisition of Fig.5, that would be obtained without using any energy threshold criterion. In the latter image the voxel are displayed also on those parts of the B-scan image where reflections from the thread phantom are not present corresponding to a low backscattered energy level. As analysed by Hoskin (Hoskin, 1997) the settings of the amplifier gain of the echograph and the energy threshold influence the system spatial resolution. In the case of Fig.5 these settings were determined in order to achieve the best fit of the velocity map morphology with the B-mode image

of the thread phantom. The developed visualization software calculates and displays in real-time the energy map of the scanned area: Fig.7 shows the normalized energy map relative to the acquisition of Fig.5 and the corresponding threshold S0.

4. System design and characteristics

The described 2D PW Doppler technique was implemented by means of a commercial echographic equipment (ESAOTE AU-3) and a custom hardware designed to take control of the ultrasonic probe during the acquisition of the 2D PW Doppler data.

The designed hardware controls both focusing and steering of a 128 elements linear array of transducers, when the echographic equipment is set to operate in a modified mode (2D PW Doppler mode) and allows to acquire data from a user-selected region. The operations in 2D PW Doppler mode are entirely controlled by a PC. The acquisition and processing set-up in this operating mode is shown in Fig.8.

Fig.8

Data acquisition is performed by a dedicated hardware controlled by the PC, with a 12 bits, 20 MHz A/D converter. The depth of the investigated rectangular region is defined by positioning the cursor on the echographic equipment monitor and then read in by the PC. The investigated region dimensions are user-selected by means of the PC software interface. The transmitter and receivers positions along the linear array are calculated by the PC, and transferred to the echograph through Bus B (see Fig.8). The position of the receiving elements is obtained by adding a lateral displacement memorised in an EPROM to the transmitter position; this displacement is determined by the PC according to the chosen steering angle (0°,4°,8°,12°), the ultrasound velocity in the propagation medium and the currently investigated voxel depth.

Data acquisition is performed by digitising the RF signal, after amplification and analog time gating. The A/D converter performs a coherent sampling at 20 MHz: four times the central frequency, 5 MHz, of the RF signal. This allows to perform fast digital demodulation of the sampled RF signal (Calzolai et al., 1998) simply as a series of sign inversion, decimation and addition operations.

Signal integration over the gate window together with the demodulation is performed by a DSP (TMS320C50). The baseband Doppler in-phase and quadrature signals are then transmitted to the PC via an Enhanced Parallel Port (EPP); Doppler spectrum evaluation, centroid estimation and velocity vector calculation are performed by the PC in order to display in real-time the velocity

maps. In particular the spectral centroids are evaluated via the periodogram technique, using 50% overlapped windows. The centroid is evaluated using only the frequency components of the Doppler spectrum above a user selectable threshold. By means the software interface can also be defined a low-pass mask in the frequency domain to reject the clutter noise.

The program on the PC, designed with a multi-thread architecture, operates in real-time in Windows environment and it is written in MS Visual C++.

The software provides different graphical outputs: a real time display of in phase and quadrature time domain signals, the corresponding signal spectra, and the temporal evolution of the velocity vector module and angle for a selected voxel in the map; moreover as described in section 3, it allows real time 2D vector velocity map display.

For real time map display, the frame rate FR can be evaluated using the following equation:

$$FR = 1/(Tacq + Tproc + Tdispl) \quad (7)$$

Where Tacq is the acquisition time of data for a complete velocity map, Tproc is the processing time for FFT, spectral centroids estimation and velocity vector calculation, Tdispl is the time required for visualization. For example, a 1x3 voxel map obtained with multigating, with 13.3 kHz PRF, 256 burst, 5 overlapping windows periodogram, is displayed at 16 frame per seconds.

The software provides also numerical outputs; in particular it can display statistical parameters (mean value and standard deviation) of the magnitude and angle of the velocity vector for a selected voxel.

An audio output of the demodulated signal coming from a pre-selected voxel is also generated, using a Sound Blaster board and Direct Sound software library.

5. Experimental results

Some experiments were performed on laboratory test-objects to produce images in real-time showing the vector velocity maps with the visualization methods described in section 3. These tests were intended to verify the system capabilities to reproduce velocity fields with known characteristics: a cotton thread test object and a rotating disc with scattering surface were used. With these test-objects it is easier to analyze the effect of the several parameters that control the acquisition, processing and visualization of the 2D velocity maps. Pulsatile flow test-objects were avoided at this stage of the research because they provide less repeatable velocity fields. Finally in

this section is reported the result of a preliminary *in vivo* experiments on the human carotid artery that show the blood flow characteristics with the vector colour coded map on a transverse section.

In Figure 9 the geometrical description of an experiment with a Doppler thread phantom realized with a cotton thread is shown.

This phantom was described in a previous work (Calzolai et. al. 1997) and it showed a good accuracy in controlling the thread velocity (within 1% in the range 0.05 m/s-1.2 m/s). The uncertainty on the angle α is better than $\pm 0.25°$ in the range 45°-135°. As described in the previous section, the software interface allows to visualize real-time images of velocity maps and also statistical parameters about the vector reconstruction on each voxel.

Results in Tables I and II are examples of acquisitions on a rectangular area with a constant thread velocity equal to 0.665m/s at angles α equal to 70° and 110° respectively: the system was programmed to investigate a map with dimensions 18x8 mm formed by $N_{VOXEL}=5x4=20$; the data acquisition was performed with PRF=13.3 kHz, 256 burst for each receiver. The multigate technique was used to estimate the velocity for two voxels simultaneously: the corresponding acquisition time for a pair of voxels is $T_{multigate}=2x256/PRF=38.5$ ms. Hence the whole map was acquired in $T_{multigate} \times N_{VOXEL}/2=385$ ms.

For each voxel four statistical data are provided: the average angle and module of the velocity vector and the corresponding standard deviations. The statistical parameters were calculated on 20 repeated measurements.

In Tables I and II are reported the numerical results for all the voxels in the maps, whose horizontal position and depth are indicated in the top row and the first column of the table.

In Fig.10 and Fig.11 are shown the visualisations of these maps according to the technique described in section 3. The velocity map (a) on the left and the energy map in gray scale on the right (b) are reported with their relative colorbar scales. The "active" voxels are determined with the energy threshold applied to the signals from both receivers; in Tables I and II these pixels are outlined with a grey background.

Velocity Module Average [m/s]	Velocity Module Std Dev. [m/s]
Angle Average	Angle Std. Dev.

Legend for Tables I and II: each sector of the table defined by thick lines is divided into four quadrants which contain the statistical data defined in the legend.

	X=0.0mm		X=3.6mm		X=7.2mm		X=10.8mm		X=14.4mm	
Z=	0.1677	0.0618	0.5150	0.1789	0.2641	0.0979	0.4405	0.1847	0.4546	0.1572
20mm	23.55	45	57.02	34.46	47.72	21.94	57.54	33.8	72.35	7.78
Z=	0.7505	0.0602	0.3035	0.2153	0.1821	0.0647	0.2507	0.0941	0.2051	0.0924
22mm	72.56	1.67	42.90	38.59	41.13	24.91	30.25	42.97	25.52	44.17
Z=	0.7274	0.1437	0.7145	0.0637	0.5399	0.1491	0.2968	0.1759	0.2079	0.0941
24mm	69.90	10.47	71.65	1.88	72.13	6.28	50.72	20.92	18.12	37.38
Z=	0.2652	0.0384	0.7179	0.0363	0.6452	0.0646	0.6546	0.1340	0.2074	0.0825
26mm	2.08	29.40	70.81	1.73	69.25	2.29	69.17	4.59	47.84	20.90

Table I. Measurements obtained from an experiment with a thread angle α=70° and nominal velocity 0.665 m/s. Active voxels are outlined with gray background and correspond to the voxels shown in Fig.10.

	X=0.0mm		X=3.6mm		X=7.2mm		X=10.8mm		X=14.4mm	
Z=	0.4366	0.2273	0.5256	0.2973	0.2390	0.1031	0.2632	0.1493	0.3163	0.1463
24mm	19.97	108.02	74.80	79.20	33.32	121.76	99.02	78.75	105.19	55.03
Z=	0.2801	0.2677	0.3382	0.2268	0.2609	0.1419	0.6027	0.1947	0.7097	0.0221
26mm	30.01	126.10	99.58	72.63	12.67	126.40	93.28	47.78	108.55	0.96
Z=	0.3235	0.1746	0.1745	0.0706	0.5972	0.0595	0.5969	0.0373	0.6946	0.0533
28mm	-78.02	2.77	64.55	117.58	113.37	3.05	112.64	1.45	110.57	1.67
Z=	0.3374	0.1089	0.6811	0.0584	0.6182	0.0393	0.5957	0.0554	0.2546	0.0363
30mm	90.68	55.21	109.78	2.01	111.89	2.01	115.35	2.77	-58.41	2.77

Table II. Measurements obtained from an experiment with a thread at inclination α=110° and nominal velocity 0.665 m/s. Active voxels are outlined with grey background and correspond to the voxel shown in Fig.11.

Another method to generate a known velocity field is the implementation of the angular velocity law ($v = \omega r$) by using a rotating disk phantom with a scattering surface. A rotating disk phantom was developed and tested in a previous work (Calzolai et al.1997): the angular velocity of the disk was varied in the range 1.5-25 rad/s with accuracy better than 1%. The disk, covered with fine sandpaper to have a uniform scattering, has a radius R=65 mm.

In our experiments a small angle φ between the disk plane and the linear probe scanning plane was used in order to minimize the non detectable velocity component orthogonal to the scanning plane (See Figure 12).

The alignment between the probe and the disk phantom was carried out by using the echograph imaging in B-mode and CFM modality. A complete description of the experiment geometry is shown in Figure 12. The scanned rectangular region on the surface of the disk phantom consists of $N_{VOXEL}=9x9=81$, which cover a 18mm x 9 mm area. The data acquisition was performed with PRF=13.3 kHz and 128 burst for each receiver. The multigate technique was used to acquire data from 3 voxels simultaneously, corresponding to $T_{multigate}=2x128/PRF= 19.2$ ms. Hence the acquisition of the whole map takes $T_{multigate} \times N_{VOXEL}/ 3=520$ ms. In spite of this time being high compared to the stationarity time of blood flow, it is appropriate for the acquisition on the disk phantom which rotates at constant velocity. This time could be reduced either by increasing the number of voxels acquired with the multigate technique, or by reducing the number of bursts transmitted for each acquisition with a detriment of accuracy of the velocity estimate.

The resulting velocity map, obtained with the disk rotating at angular velocity $\omega=20.5$ rad/s, is shown on the left side of Figure 13 along with the color-bar of the velocity module scale. As it can be observed in the Figure 13, the estimated velocity map reproduces the expected distribution of the velocity field in the scanned area.

The system was tested *in vivo* on the left common carotid artery (CCA). In Figure 14 it is shown a vector velocity map of a single line of sight consisting of three voxels in the vessel, acquired in multigate, superposed to the B-mode echographic image.

The system is also capable to show in real-time other information relative to the acquired signals. In particular we believed useful for the diagnosis to show the Doppler spectra, the velocity module and angle for a single voxel selected on the vector velocity map. In this kind of visualisation, the temporal diagrams of the velocity module and angle are inspired by other common representations of biomedical instruments as ECG or Doppler sonograms: here the time evolution of the velocity module and angle relative to the selected voxel in the map is displayed. This can be a useful tool for the physician to extract the quantitative information contained in the velocity map.

References

D.H. Evans,W.M. McDicken, R. SkidMore, J. P. Woodcock "*Doppler Ultrasound - Physics, Instrumentation, and Clinical Application*", Chichester, England: Wiley, 1989

Mohiaddin RH, Yang G.Z., Kilner P.J., Visualization of flow by vector analysis of multidirectional cine MR velocity mapping. J Comput Assist Tomogr, 1994: 18: 383-392

J. R. Overbeck, K. W. Beach, "*Vector Doppler: accurate measurement of blood velocity in two dimensions*", Ultrasound in medicine and biology, vol. 18, no. 1, pp. 19-31, 1992

I. A. Hein, "Three-dimensional blood flow velocity vector estimation with a triple-beam ultrasonic lens", *Ultrasonics Symp. Proc.*, 1994, pp.1737-1742.

G. Bruni, M. Calzolai, L. Capineri, A. Fort, L. Masotti, S. Rocchi, M. Scabia, "*Measurement and imaging of a velocity vector field based on a three transducer Doppler system*", Acoustical Imaging, vol. 22, 1995, Ed. by P. Tortoli and L. Masotti, Plenum Press, New York and London, pp. 431-438

M. Calzolai, L. Capineri, A. Fort, L. Masotti, S. Rocchi, M. Scabia; "*Analysis of factors influencing the accuracy of a 3D PW Doppler technique: simulations and experimental results*", 1996 IEEE International Ultrasonics Symposium, San Antonio, Texas, USA, Nov.3-6, 1996

V. L. Newhouse, D. Censor, T. Vontz, J. A. Cisneros, H. V. Ortega, "*Ultrasound Doppler probing of flows transverse with respect to beam axis*", IEEE transactions on biomedical engeneering, vol. BME-34, pp. 779-789, Oct. 1987

J.A. Jensen and P. Munk, A new method for estimation of velocity vectors, IEEE transactions on UFFC, Vol. 45, N.3, 837-851,1998

G. E. Trahey, J. W. Allison, O. T. Von Ramm, "Angle independent ultrasonic detection of blood flow", *IEEE Trans. Biomed. Eng.*, vol. BME-34, pp. 965-967, Dec. 1987.

Von Ramm, O.T.; Smith, S.W.; Pavy, H.G. High-speed ultrasound volumetric imaging system. Part I and II. IEEE Trans. Ultrason. Ferroelect. Freq. Cont. 38: 100-115; 1991.

Masotti, L.; Pini, R. Three-Dimensional Imaging. In: Wells P.N.T. ed. Advances in Ultrasound Techniques and Instrumentation. New York: Churchill Livingstone; 1992: 69-77.

Pini, R.; Costi, M.; Masotti, L.; Greenberg, K.L.D.P.; Greppi, B.; Cerofolini, M.; Devereux, B. Three-Dimensional (3D) acquisition and display of be heart echo image. In: Yu Wey and Benli Gu ed. Acoustical Imaging vol.20. New York: Plenum; 1993: 425-430.

R. Shandas, C.G. DeGroff, J. Kwon, N. Trujillo, E.A. Gill, L. Valdes-Cruz,Utility of three-dimensional ultrasound Doppler flow reconstruction of the proximal jet to quantify effective orifice area: in vitro steady and pulsatile flow studies. Journal of America Society of Echocardiography, Vol. 11, N.4, April 1998, pp 313-321.

C. D. Emery and S.W. Smith, Improved Signal to noise ratio in hybrid 2-D arrays: experimental confirmation, Ultrasonic Imaging, 19, 93-111, (1997)

M. Calzolai, L. Capineri, A. Fort, P. Lucetti, L. Masotti , M. Scabia
Real-time digital demodulation technique for ultrasonic Doppler signal
Alta Frequenza-Rivista di Elettronica Vol.10, N.2, Marzo Aprile 1998, pp. 51-55

Katherine Ferrara, Gia DeAngelis "*Color Flow Mapping*", Ultrasound in Medicine & Biology, Vol.23, No.3 , pp 321-345, 1997

A. V. Oppenheim, R. W. Shafer, "*Elaborazione numerica dei segnali*", Ingegneria elettrica Franco Angeli, 1985.

S. Li, P.R.Hoskins and W.N. McDicken, Rapid measurement of the spatial resolution of colour flow scanners, Ultrasound in Medicine & Biology, Vol.23, No.4 , pp 591-596, 1997

P. R. Hoskins "*Peak Velocity Estimation in arterial stenosis models using color vector doppler*", Ultrasound in Medicine & Biology, Vol.23, No.6 , pp 889-897, 1997

Theofanis A. Maniatis, Richard S,C. Cobbold, Wayne Johnston *"Flow imaging in an end-to-side anastomosis model using two-dimensional velocity vectors"*, Ultrasound in Medicine & Biology, Vol.20, No.6 , pp 559-569, 1994

Ding-Yu Fei, Cai-Ting Fu, William H. Brewer, Kenneth A. Kraft *"Angle indipendent doppler color imaging : determination of accuracy and a method of display"*, Ultrasound in Medicine & Biology, Vol.20, No.2 , pp 147-155, 1994

N.Vera, D.A.Steinman, C.R. Ethier, K.W. Johnston, R.S.C Cobbold *"Visualization of complex flow fields, with application to the interpretation of colour flow doppler images"*, Ultrasound in Medicine & Biology, Vol.18, No.1 , pp 1-9, 1992

Charles, R.D. Viewing velocity in flow fields, ASME Mechanical Eng. 111(8):64-67;1989

M. Calzolai, L. Capineri, A. Fort, L. Masotti, S. Rocchi, M. Scabia
A 3D doppler scanning system for quantitative flow measurements
in Acoustical Imaging,Vol. 23, Edited by S. Lees,and Leonard A. Ferrari, Publ. Plenum Press, New York and London, 1997, pp.285-290

Phillips P.J., Straka S.W., von Ramm O.T., Ultrasonic Imaging, 18:60, 1996

Figures

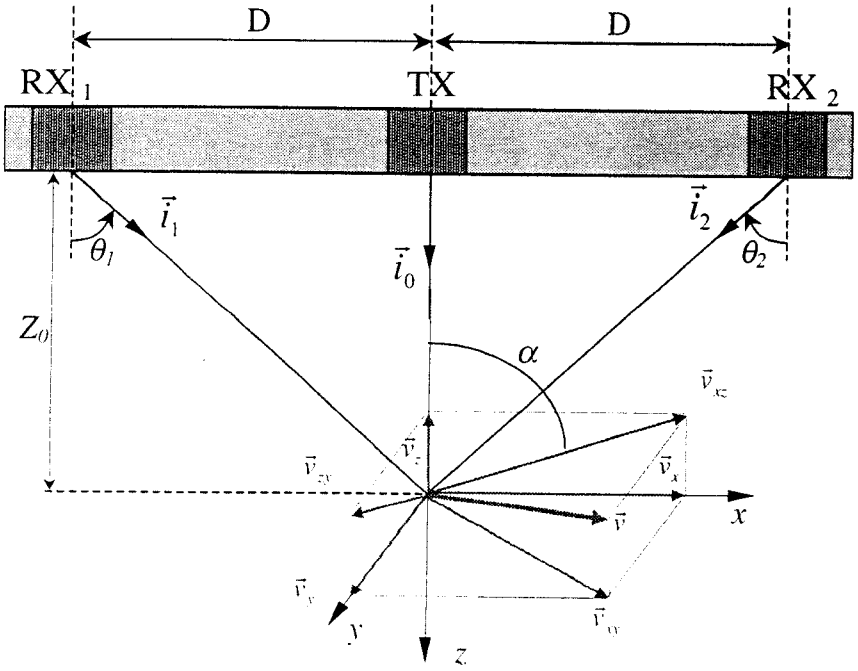

Figure 1

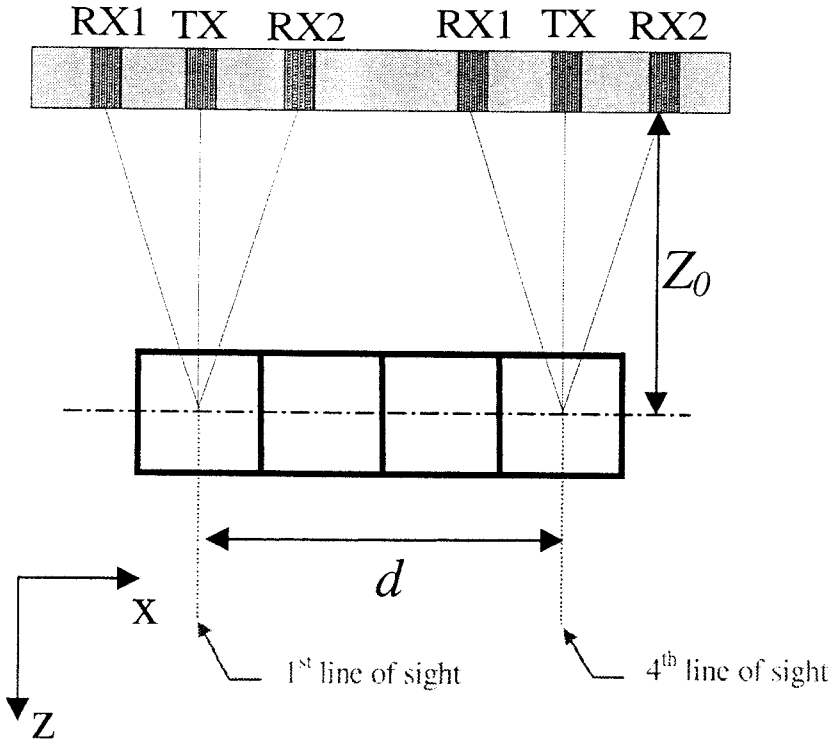

Figure 2

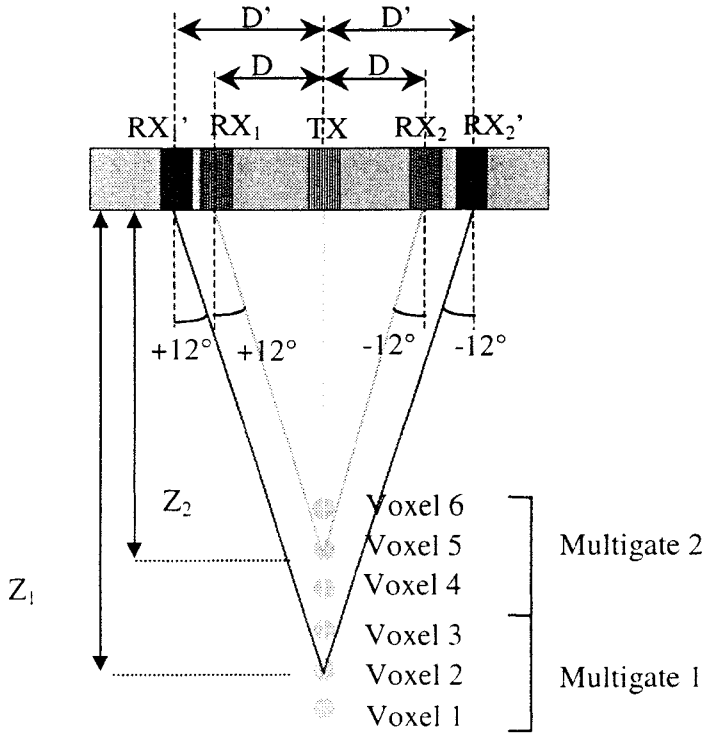
D'
D'
D
D
RX1'
RX1
TX
RX2
RX2'
+12°
+12°
-12°
-12°
Z2
Z1
Voxel 6
Voxel 5
Voxel 4
Voxel 3
Voxel 2
Voxel 1
Multigate 2
Multigate 1

Figure 3

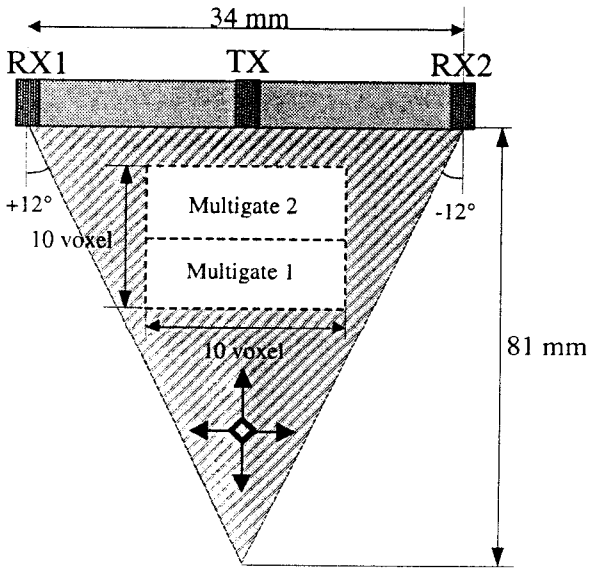

Figure 4

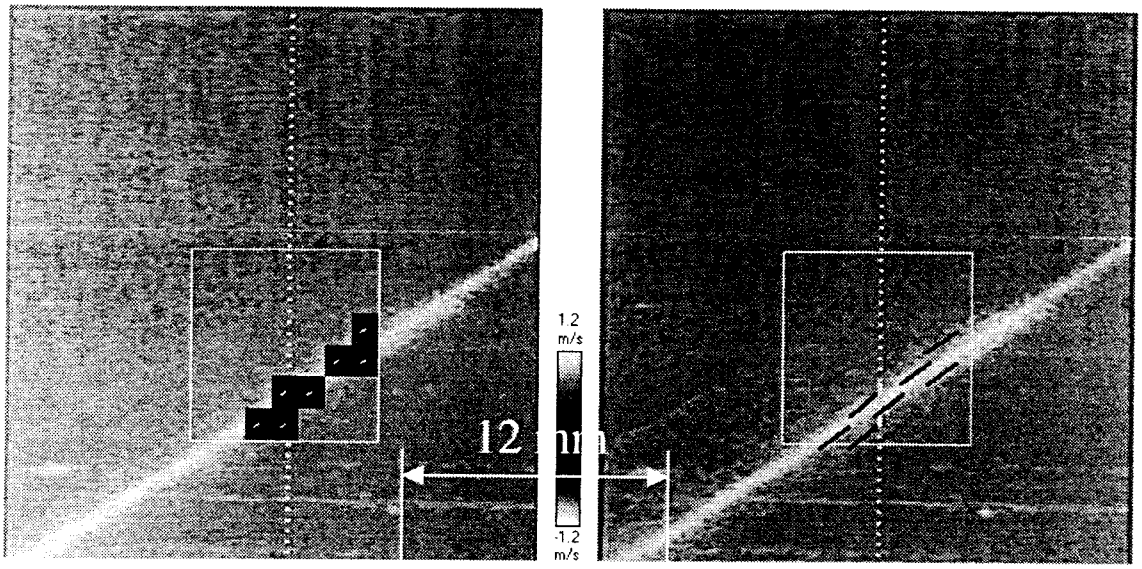

Figure 5a

Figure 5b

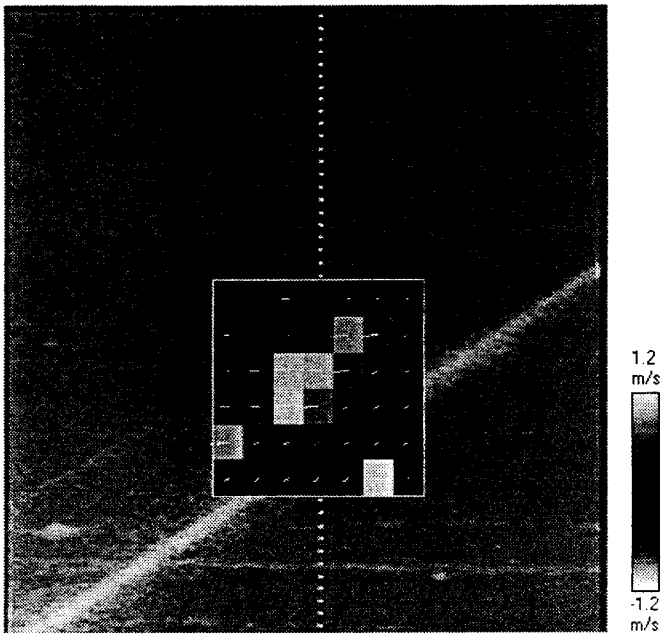

Figure 6

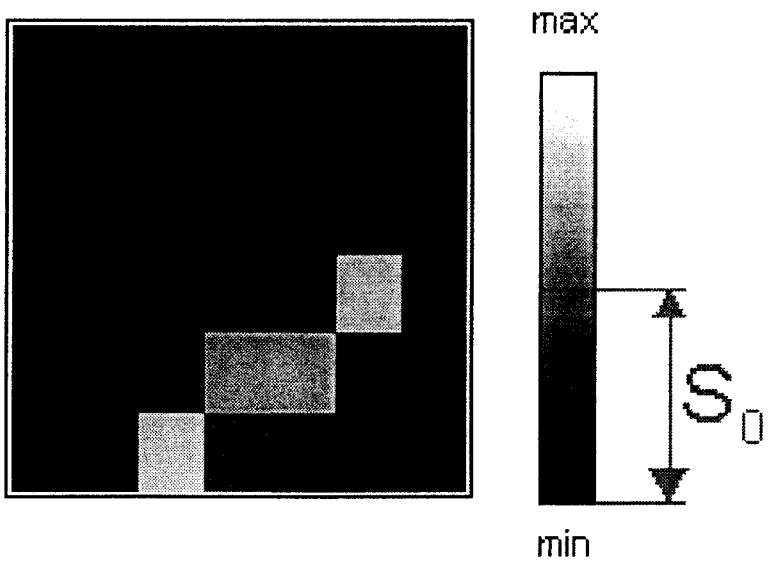

Figure 7

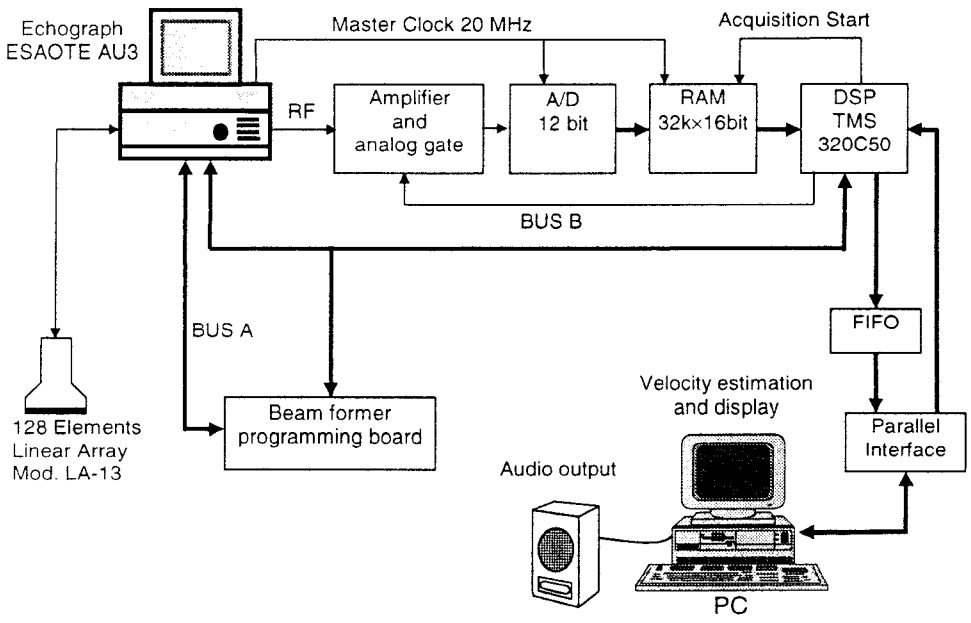

Figure 8

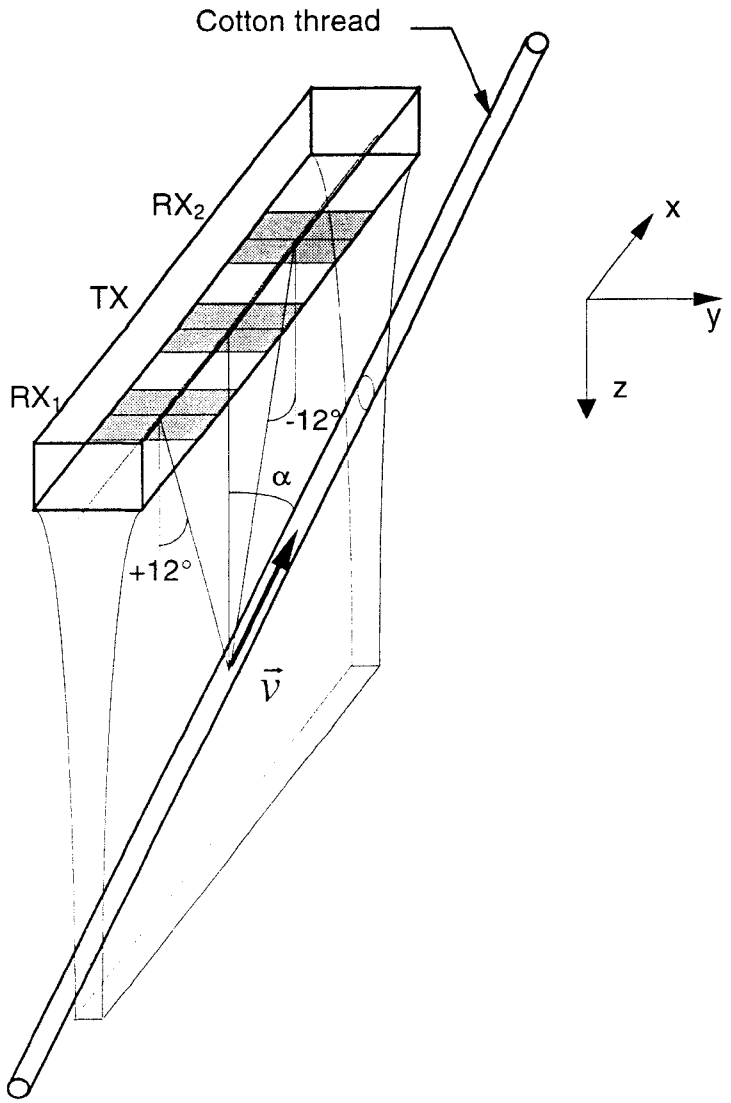

Figure 9: Schematic drawing of the experimental set-up for the acquisition of a velocity map on a cotton Doppler thread phantom. The thread lies on the linear array probe scanning plane and has an orientation angle α with respect to the axis z. $\vec{V}$ is the velocity vector of the examined volume selected by the electronic focusing system.

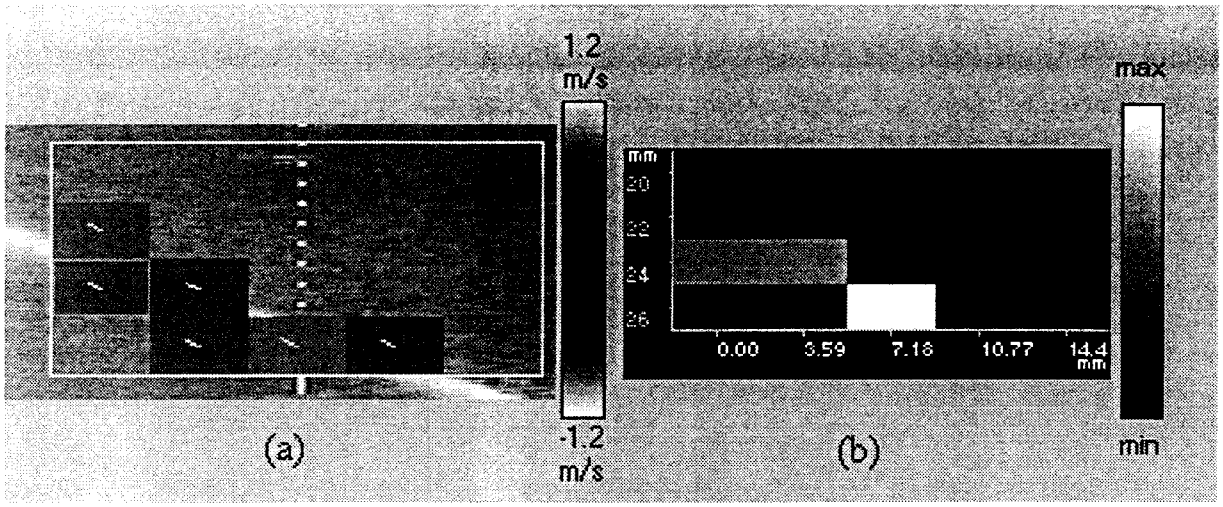

Figure 10: Velocity map 5 x 4 voxel ; (b) Energy map. Thread inclination α=70° and velocity 0.665 m/s.

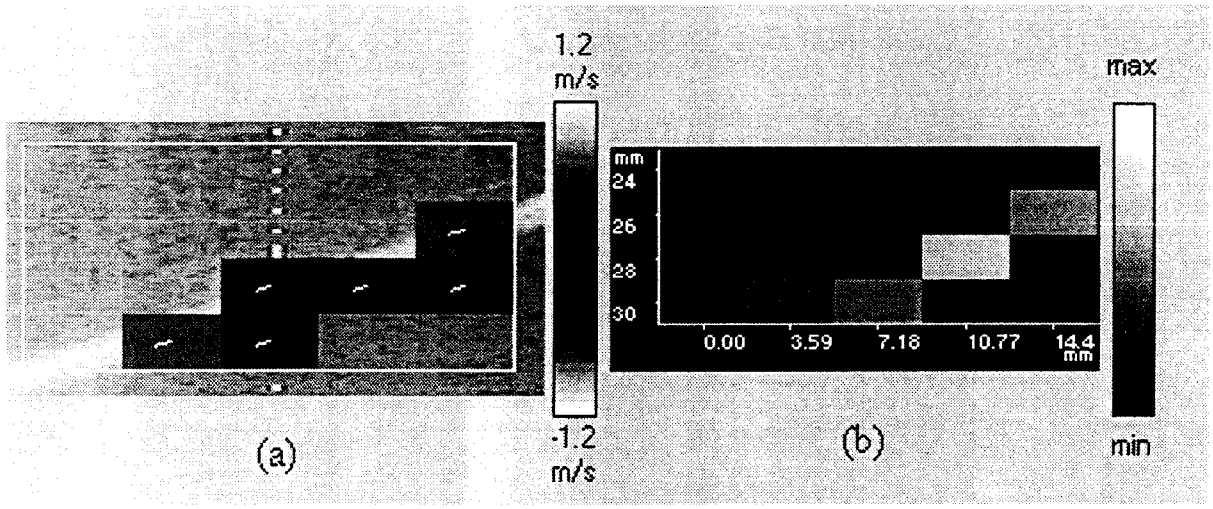

Figure 11: Velocity map 5 x 4 voxel ; (b) Energy map. Thread inclination α=110° and velocity 0.665 m/s.

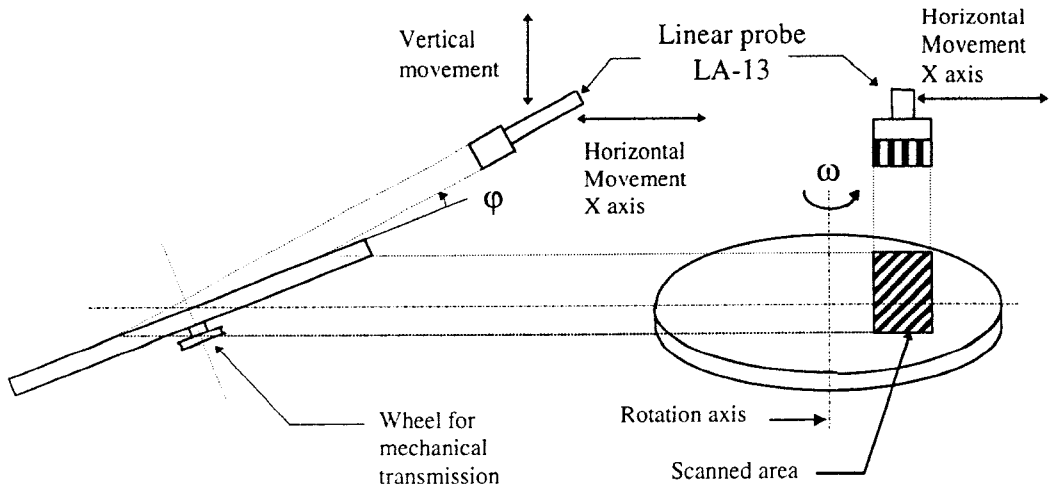

Figure 12: Experiment geometry with a rotating disk covered with glass paper and immersed in water. The scanned area is displayed with a highlighted rectangle. The length of the scanned area is obtained by tilting the disk with respect to the horizontal position. The probe scanning plane and the disk plane form a small angle φ.

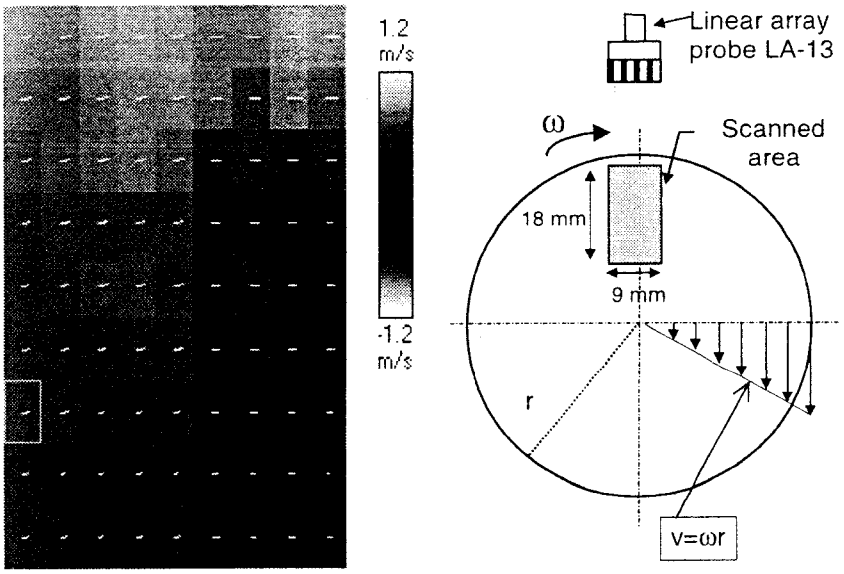

Figure 13: On the left: velocity map of 9 × 9 voxels relative to the scanned area over the disk phantom. On the right: position of the scanned rectangular area, 18mm x 9 mm, on the surface of the disk phantom. The disk phantom, with radius r=65 mm, had angular velocity ω=20.5 rad/s. As it can be observed in the velocity map, the scanned area contains voxels with both velocity towards (red) and away (blue) from the linear array probe and the estimated velocity modules increase with the radial distance (angular velocity law).

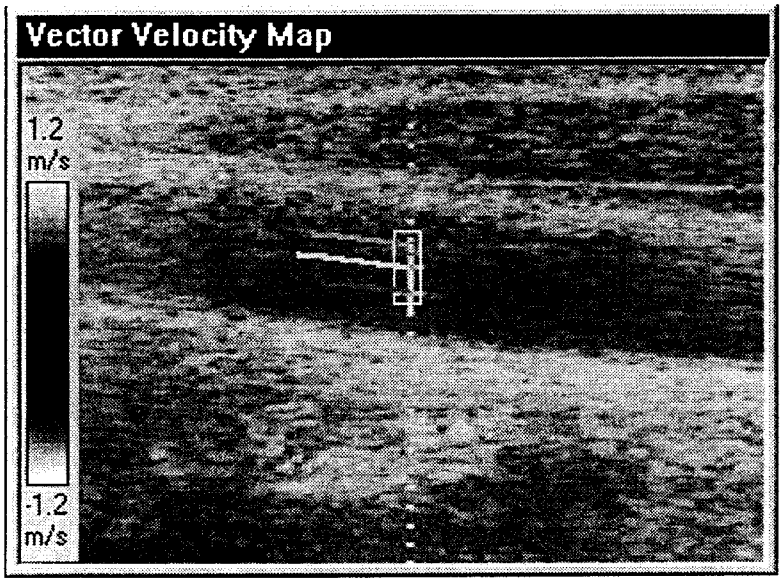

Figure 14